We are IntechOpen, the world's leading publisher of Open Access books Built by scientists, for scientists

6,900
Open access books available

186,000
International authors and editors

200M
Downloads

154
Countries delivered to

Our authors are among the

TOP 1%
most cited scientists

12.2%
Contributors from top 500 universities

CLARIVATE ANALYTICS
BOOK CITATION INDEX
INDEXED

WEB OF SCIENCE™

Selection of our books indexed in the Book Citation Index
in Web of Science™ Core Collection (BKCI)

Interested in publishing with us?
Contact book.department@intechopen.com

Numbers displayed above are based on latest data collected.
For more information visit www.intechopen.com

UHF Tags for Sensing Applications

Gaetano Marrocco
University of Roma Tor Vergata
Italy

1. Introduction

The recent advances in Wireless Sensor Networks (WSNs) (Kong & Kumar, 2003) for applications in mobile and time-varying environments are generating a growing attention to low-cost and low-power wireless nodes, equipped with radio/sensing ability, which are spatially distributed to ensure a cooperative monitoring of physical or application-specific conditions and parameters. Typical fields of applications for WSNs include environmental and habitat monitoring, disaster relief (Lorincz et al., 2004), health care, inventory tracking and industrial processing monitoring, security and military surveillance, smart spaces applications. A novel technological trend is the integration among wireless sensor networks and Radio Frequency IDentification (RFID) technologies. Such a convergence of sensing and identification features may enable a wide range of heterogeneous applications which demand a tight synergy between detection and tagging.

A new frontier is the wireless monitoring of people within Mobile Healthcare Services (Cheng-Ju et al., 2004) with the purpose to reduce the hospitalization of patients, to support disaster relief or to get an epidemic under control. An RFID system could provide real-time bio-monitoring and localization of patients inside hospitals or domestic environments, as well as in extreme conditions like a Space Capsule. In these cases the tag should be placed on the human body and equipped with bio-sensors (temperature, blood pressure, glucose content, motion) and, when activated by the reader, tag ID and bio-signals could be transferred to a remote units and then stored and processed.

Up to date, several approaches have been proposed to provide RFID devices with enhanced sensing and detection capabilities. The main solutions make use of active or passive RFID transponders and Surface Acoustic Wave (SAW) devices (Reindl et al., 2001). A significant example of enhanced passive RFID system is given by the Wireless Identification Sensing Platform (WISP) project (Sample et al., 2007) which introduced the concept of ID modulation making use of inertial switches and enhanced power harvesting units to mechanically toggle between two commercial RFID integrated circuits.

These devices could be *passive*, harvesting energy from the interrogating system, *semi-active* when a battery is included only to feed the sensors, or fully *active* where a local source directly feeds a microcontroller beside the transmitting radio. However, the large battery packs required for active techniques, in addition to the use of protruding antennas, could be suboptimal for some applications and additional issues have to be considered such as the compromise between a long battery-life and a miniaturized design.

In passive RFIDs, together with the microchip sensitivity, the tag antenna plays a key role in the overall system performance, such as the reading range and the compatibility with the tagged object. In case of RFID with sensing capability, the antenna should be additionally suited to electrical and physical integration with sensing electronics. Moreover, it is well experienced that the RFID system's performances are greatly dependent on the kind of object where the tag is attached on. When a same tag is placed onto different targets, the tag antenna's input impedance may in some case undergo a mismatch and may produce a change of the read distance. Conventional general-purpose tags are designed in free space, but when they are needed to be applied over objects having high values of the permittivity, as in the case of liquids and humans, the strong pattern distortion and the efficiency loss caused by energy dissipation and scattering, have to be taken into account in the first stage of the design.

Within this scenario, this chapter has a twofold purpose: the description of a new class of UHF tag layouts suited to host sensors and to be attached onto high dielectric and lossy targets, such as the human body, and to introduce the novel concept of *self-sensing* tags wherein the antenna itself acts both as a data transmitter and as a sensing device of some tagged body's features. These two arguments are both related to the modelling and handling of *dense* objects, and the *self-sensing* idea originates just from one of the main conventional drawbacks of UHF RFID, e.g. the dependence of reading performances on the dielectric value of the tagged object. The self-sensing tags are multi-chip antennas (multi-port system) exploiting the dependence of the tag's input impedance and radar cross-section on the physical and geometrical features of a real target.

The two subjects are here described both theoretically and corroborated by several preliminary prototypes and experimentations.

2. Basic definitions for RFID systems

At the beginning of the reader-to-tag communication protocol (Nikitin & Rao, 2006), the reader first *activates* the tag, placed over a target object, by sending a continuous wave which, on charging an internal capacitor, provides the required energy to perform actions. During this *listening mode*, the microchip (IC) exhibits an input impedance $Z_{chip} = R_{chip} + jX_{chip}$, with X_{chip} capacitive, and the antenna impedance $Z_A = R_A + jX_A$ should be matched to Z_{chip} ($Z_A = Z_{chip}^*$) for maximum power transfer. The maximum fraction $P_{R \to T}$ of the reader input power that is absorbed by the tag is

$$P_{R \to T} = \left(\frac{\lambda_0}{4\pi d} \right)^2 G_R \tau G_T P_{in} \tag{1}$$

$$\tau = \frac{4 R_{chip} R_A}{\left| Z_{chip} + Z_A \right|^2} \tag{2}$$

where λ_0 is the free-space wavelength, d is the reader-tag distance, G_R is the gain of the reader antenna and G_T is the gain of the tag over the target, having assumed polarization-matched antennas aligned for maximum directional radiation. τ is the power

transmission coefficient. The tag is activated when the absorbed power exceeds the tag's microchip sensitivity threshold: $P_{R \to T} > p_T$. Having fixed the effective power ($EIRP_{R=}G_R P_{in}$) transmitted by the reader, the tag antenna gain (G_{tag}) and the sensitivity (P_{chip}) of the tag microchip, e.g. the RF power required to the microchip electronics to turn on and complete its tasks, the maximum activation distance of the tag along the (θ,ϕ) direction is therefore given (Nikitin & Rao, 2006) by

$$d_{\max}(\theta,\phi) = \frac{c}{4\pi f}\sqrt{\frac{EIRP_R}{P_{chip}}\tau G_{tag}(\theta,\phi)} \qquad (3)$$

During the next steps of the communication, the tag receives the command coming from the reader and it finally sends back the data through a back-scattered modulation of the continuous wave coming from the reader itself. The tag's IC acts as a programmable switching device which toggles between a low or high modulation impedances Z_{mod}. During the data transfer, the RFID system can be considered as a monostatic radar and therefore it can be characterized by the radar range equation which, for the case of typical RFID tags, can be expressed in the form

$$\frac{P_{R \leftarrow T}(d)}{P_{in}} = \left(\frac{\lambda_0}{4\pi d}\right)^4 G_R^2 G_T^2 \rho \qquad (4)$$

$$\rho = \frac{4R_A^2}{|Z_{\mathrm{mod}} + Z_A|^2} \qquad (5)$$

where $P_{R \leftarrow T}$ is the power received back by the reader and ρ is a modulation parameter related to the tag's radar cross section.

The maximum transmitted power allowed to the reader is constrained to local regulations. In Europe the relevant standards for UHF RFID applications are the ETSI EN330-220 and Draft TESI EN302 208-2. In particular within the 865.6-867.6MHz the maximum EIRP is 3.2W, which overcomes the previous limit 0.8W. In the U.S.A. the FCC allowed band is 902-928MHz with maximum transmitted EIRP=4W.

Microchip power activation threshold is continuously improving, reducing from 1mW in the year 2001 to some microwatts in today products or even less in the state of the art ASICS (Curty et al., 2005).

It is easy to show from equation (3) that antennas with averaged realized gain ($G_{tag}\tau$) not less than -10dB (when placed over the human body) could be in principle compatible with reading distances of the order of 5m if the microchip sensitivity is less than 10μW.

3. Energetic constraints for on-body RFID applications

The presence of the tagged object, and in particular of the human body, with its high permittivity and conductivity, will favour the antenna miniaturization but nevertheless will induce a strong power absorption in body tissues. The antenna gain, and hence the link distance, will be sensibly reduced with respect to the free space. Additionally, when the human body is exposed to electromagnetic field radiated by the reader, the power budget

has to comply with the Safety standards, typically expressed in the UHF band in terms of maximum power absorbed by human tissues. The reference quantity is the Specific Absorption Rate (SAR), measured in [W/Kg], e.g. the power absorbed by the mass unit:

$$SAR(\underline{r}) = \frac{1}{2\rho_{mass}(\underline{r})}\sigma(\underline{r}) \mid E(\underline{r}) \mid^2 \qquad (6)$$

where ρ_{mass} and σ are the mass-density and the electric conductivity, respectively, at point $\underline{r}$ of the body. Since the strength of electromagnetic field emitted by the reader decreases along with the distance, a *safety distance* may be introduced for the reader (having fixed the radiated power) or, from a different point of view, a *safety EIRP* when the distance is fixed. The useful link region is therefore theoretically bounded by the safety distance and the maximum range allowed by the transmitted EIRP.

To calculate the safety distance, the SAR has to be estimated by using computer simulations considering a realistic morphologic model of the human body and a simplified, but very general model of the emitted field from the reader. Although the data link could not be necessarily continuous, it is nevertheless useful to consider the extreme case of continuous interrogation, giving the maximum SAR over the period of the wave.
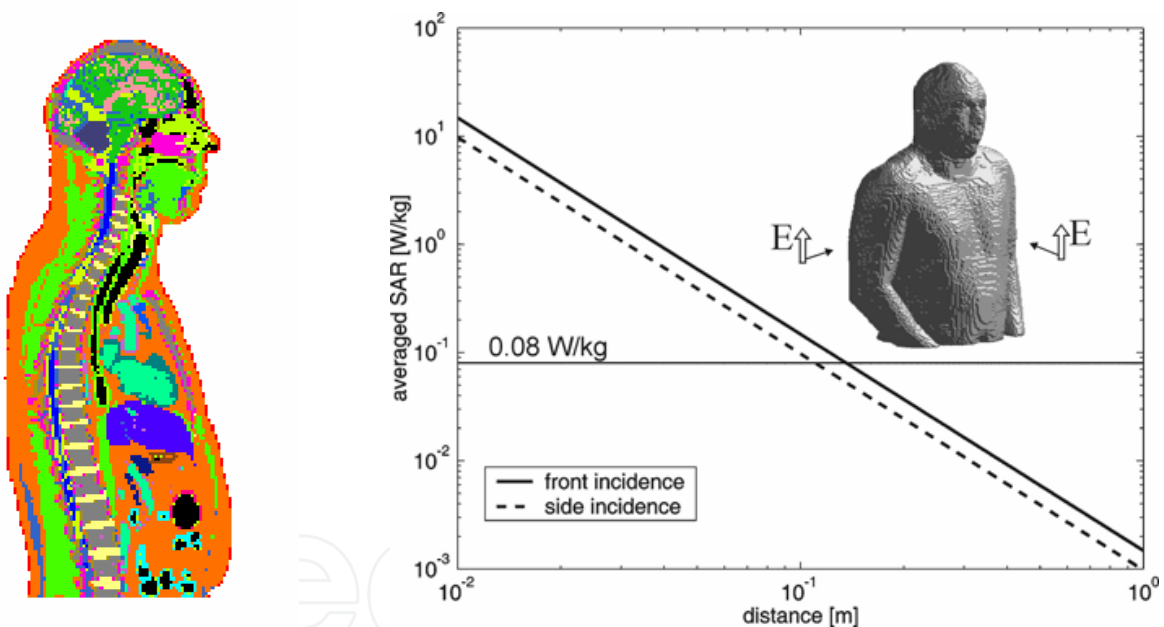

Fig. 1. Absorbed power density (SAR) in the realistic human body model exposed to a vertically polarized plane-wave coming from the reader and carrying a power 3.2W EIRP.

The voxel-based human body model used in the computer simulation has been derived by the Visible Human project (Ackerman, 1999) which comprises the thorax and the head with more than forty different tissues (Fig. 1). Physical parameters (relative permittivity ε_r, conductivity σ and mass density ρ) at 900MHz are retrieved by the tissue database in (Gabriel et al., 1996). Under the hypothesis that the human body is placed in the reader's far field, a plane wave exposure is considered. The plane wave impinging the side and the thorax carries a power density $S^{in} = EIRP_R /(4\pi d^2)$ and then the plane wave strength delivering power absorption into the human body is

$$| E^{in} |= \sqrt{60EIRP} / d \qquad (7)$$

The numerical calculation, and the required dosimetric processing were accomplished by means of the tool in (Marrocco & Bardati, 1999), based on the Finite-Difference Time-Domain (FDTD) method (Taflove, 1998).

d [m]	Imperturbed r.m.s. |E| [V/m]	Maximum SAR in the head [mW/kg]	Maximum SAR in the trunk [mW/kg]	Body averaged SAR [mW/kg]
0.1	98	331	197	148
0.2	49	84	49	37
0.5	20	13	8	6
1.0	10	3	2	1.5
2.0	5	1	1	<1
3.0	3	<1	<1	<1
4.0	2	<1	<1	<1

Table 1. Human-body front exposure to Reader's field at 900 MHz, having assumed an emitted power of 3.2W EIRP

Fig. 1 shows the SAR averaged over the whole model with respect to the tag-reader distance, for a transmitted power 3.2W EIRP and two different wave incidences (toward the thorax and toward the torso's side), while Table 1 gives the detailed values of the impinging field strength as well as of the maximum and averaged SAR. According to the European regulations, which are more restrictive than the USA ones, the maximum allowed averaged SAR in the body is 80 mW/Kg (CENELEC, EN50364). It is hence possible to observe that the smallest safety distance is about d_{min}=10cm. Even assuming a more conservative value d_{min} =50cm, this safety distance is fully compatible with the concept of remote monitoring.

4. UHF Slot-Tags for on-body application

Three tag geometries are here described together with the related design methodologies. These layouts are slot-type antennas suited to be easily integrated with sensors and additional electronics and useful for placement on high dielectric targets such as human-body districts (Fig. 2). In particular the first two antennas are useful to integrate sensors in close contact with the human body (or any other dielectric), as for the detection of pressure, glucose or temperature while the third layout is engineered for non contacting sensors, for
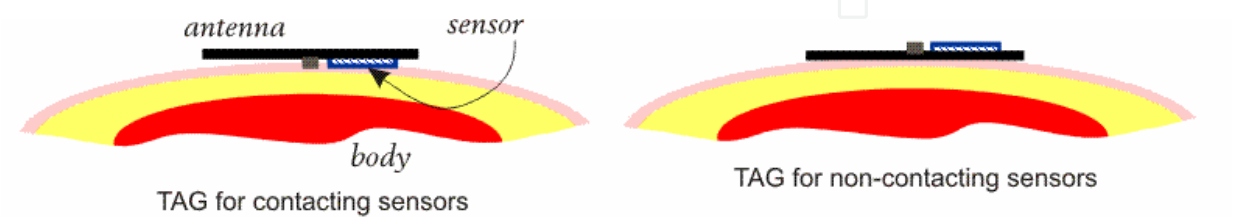

Fig. 2. Tag hosting sensor in close contact to the tagged body (temperature, pressure or chemical sensing) or shielded from it by the antenna itsself (motion-detection accelerometers).

instance accelerometers, and permits to achieve superior reading performance than the previous family.

All the presented tags are numerically modelled by the Finite-Difference Time-Domain solver as above, having considered the antenna placed onto realistic models of the tagged body.

4.1 Tags for contacting sensors

The first tag antenna family is a nested-slot suspended-patch (NSSP), (Marrocco, 2007). Small size slot antennas are naturally inductive and therefore appear more suited than dipoles to achieve conjugate impedance matching. The basic geometry is visible in Fig.3a and has been modelled as placed on a layered cylinder (Fig.3b) simulating the human torso (size and materials in Table 2). To prevent high losses on the skin, the antennas is attached onto the body through an insulating slab.
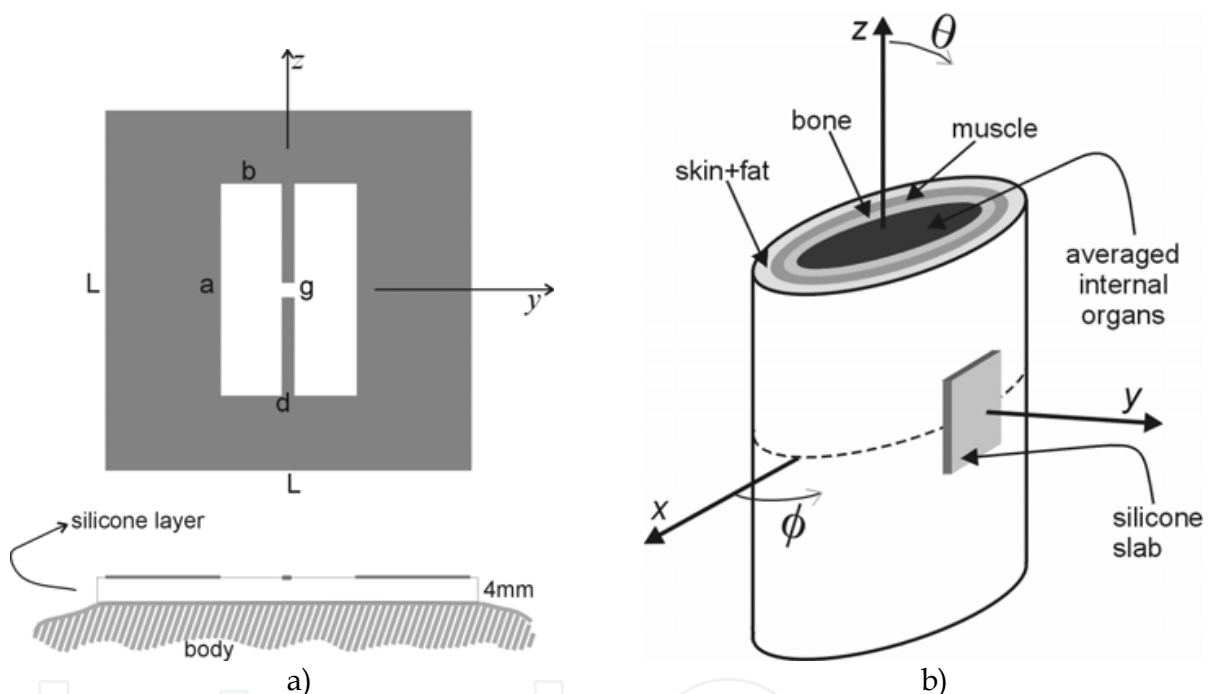
Fig. 3. a) NSSP tag: the microchip transmitter should be placed in the central gap of size g x g. b): Stratified elliptical cylinder model of the human thorax for the design of bio-compatible tags. The size of cylindrical cross-sections are reported in Table 2. Cylinder height: 40cm.

Since the slot sizes are comparable with the patch surface, the radiation features are related to both the objects. In particular, the maximum antenna gain is mainly fixed by the patch side L, while the impedance tuning can be changed by acting on the slot size a and b, as visible in the *Matching Chart* in Fig. 4a, which displays the iso-lines for antenna input resistance and reactance. Having chosen a particular microchip, this chart permits to design the H-slot shape factor such to achieve the conjugate impedance matching required for maximum reading distance.

Depending on the shape of the internal slot, the antenna mainly radiates either as a *dumbbell H*-slot or as a pair of rectangular loops sharing the sourced conductor (Fig. 4b).

Layer	ε_r	σ [S/m]	Ellipse axis *thin man* [cm]
Skin+fat	14.5	0.25	33.5×16.8
Muscle	55.1	0.93	31.0×14.2
Bone	20.8	0.33	28.4×10.5
Internal organs	52.1	0.91	27.2×8.4

Table 2. Physical and geometrical parameters of the layered anatomical model in Fig. 3 at 870MHz.
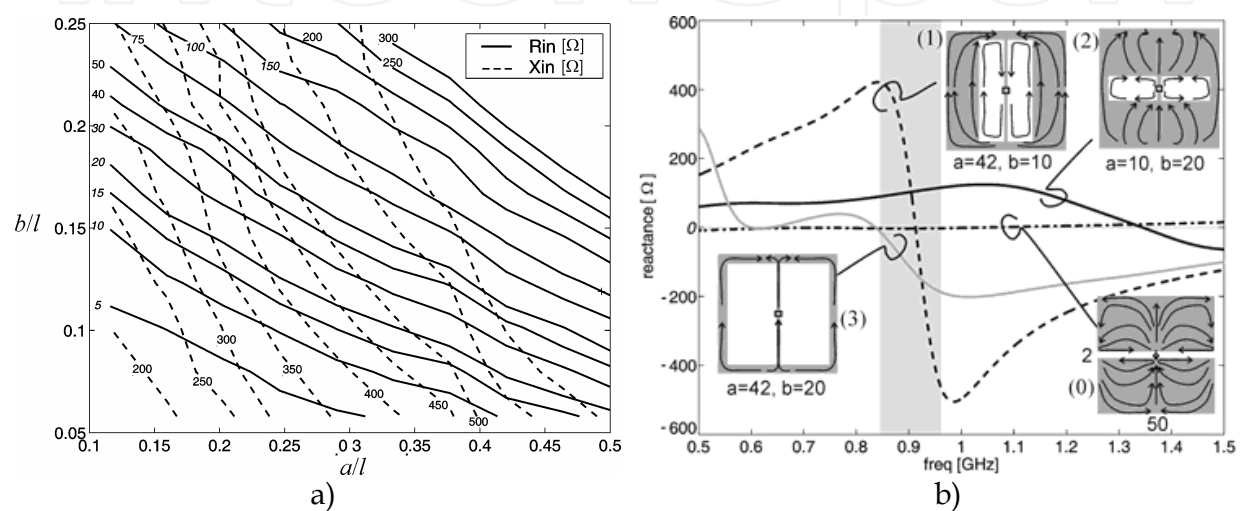

Fig. 4. NSSP tag. a) Matching chart to design the H shape factor of the antenna such to match the particular microchip's impedance. b) Typical antenna input impedance for some choice of the H-slot parameters (in mm). In all the case the patch size is L=50mm.

Fig. 5 shows a fabricated prototype of the body-matched NSSP tag and the measurement set-up where the tag is attached onto a Perspex box (ε_r=2.7, σ=0) having 5 mm thickness and 20 cm width, filled with a muscle-type solution. The measured antenna input impedance and power matching, compared with simulations, are shown in Fig. 6. The experiment demonstrated a significant impedance tuning agility and a read region (Fig. 7) suited to small or even medium-size rooms.

The previously considered NSSP antennas are symmetric with respect to both the x and z axis. However, this geometry offers additional degrees of freedom in the position of the slot and in the connection to the microchip, provided that a larger number of slot discontinuities (Fig. 8a) are considered. This new layout is similar to a meandered slot and, when properly optimized, could permit to fulfill several electrical and geometrical constraints, such as the impedance matching to a particular microchip, dual-frequency operations, the embedding of a sensor of given size, and a stable response over a large variety of tagged dielectrics. The slot profile can be seen as a slot-line impedance transformer (Calabrese & Marrocco, 2008), where each discontinuity (tooth) provides energy storage and radiation. A Genetic Algorithm (Weile & Michielsen, 1997) optimization problem is hence formulated to shape the transformer layout, within input impedance and size requirements. As an example, Fig.8b shows the shape and the power transmission coefficient τ for some 870MHz slot-line antennas optimized to occupy only a fraction of the overall metallization. A preliminary

experimental prototypes on FR4 has been fabricated and measured (Fig. 9). When compared with the NSSP tags, this layout permits to achieve a better gain and more space for the electronic payload.
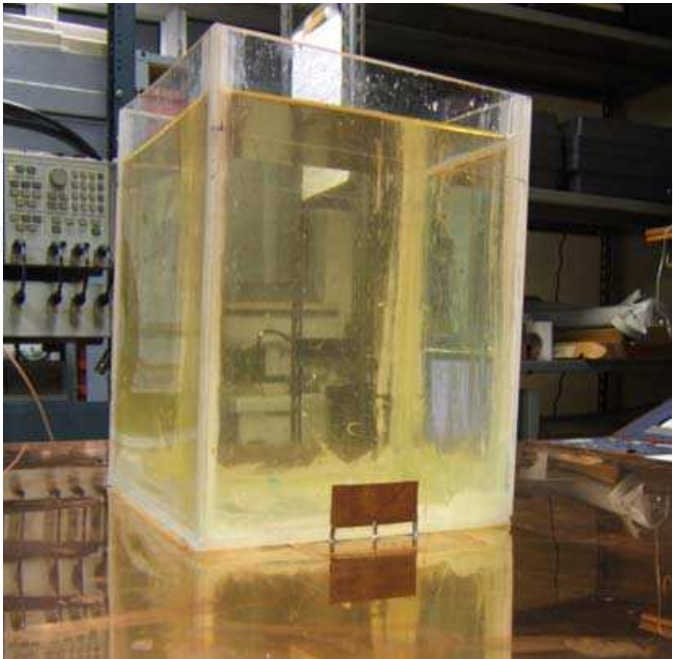

Fig. 5. NSSP tag. Fabricated half--NSSP antenna in front of a Perspex cubic phantom filled with tissue-equivalent solution made of deionised water, saccharose and sodium chloride. The antenna and the box are placed over a 1m x 1m copper image plane simulating, by image effect,the other half structure.
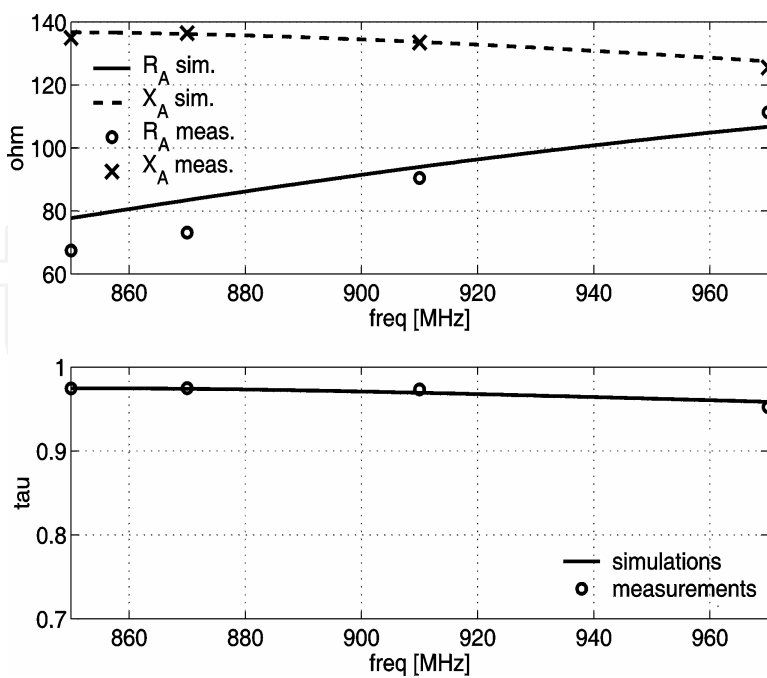
Fig. 6. NSSP tag. Measured and computer-estimated input impedance and power transmission factor τ.
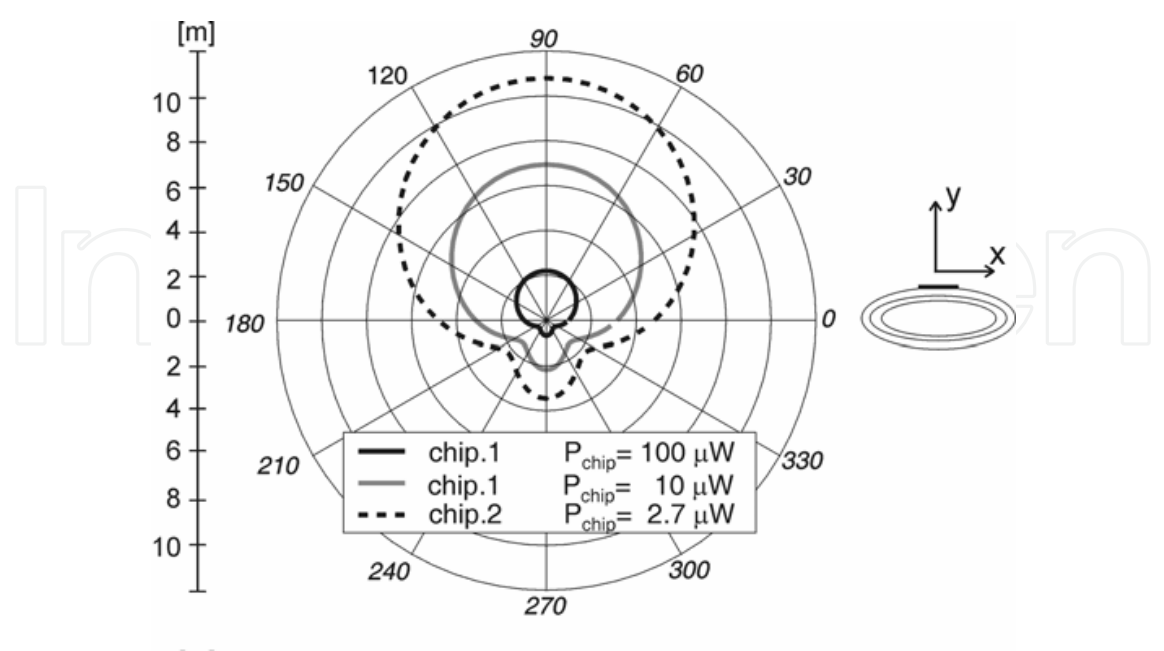
Fig. 7. NSSP tag. Estimated read distance for different kinds of microchip and 3.2 W EIRP emitted power.

a)

b)
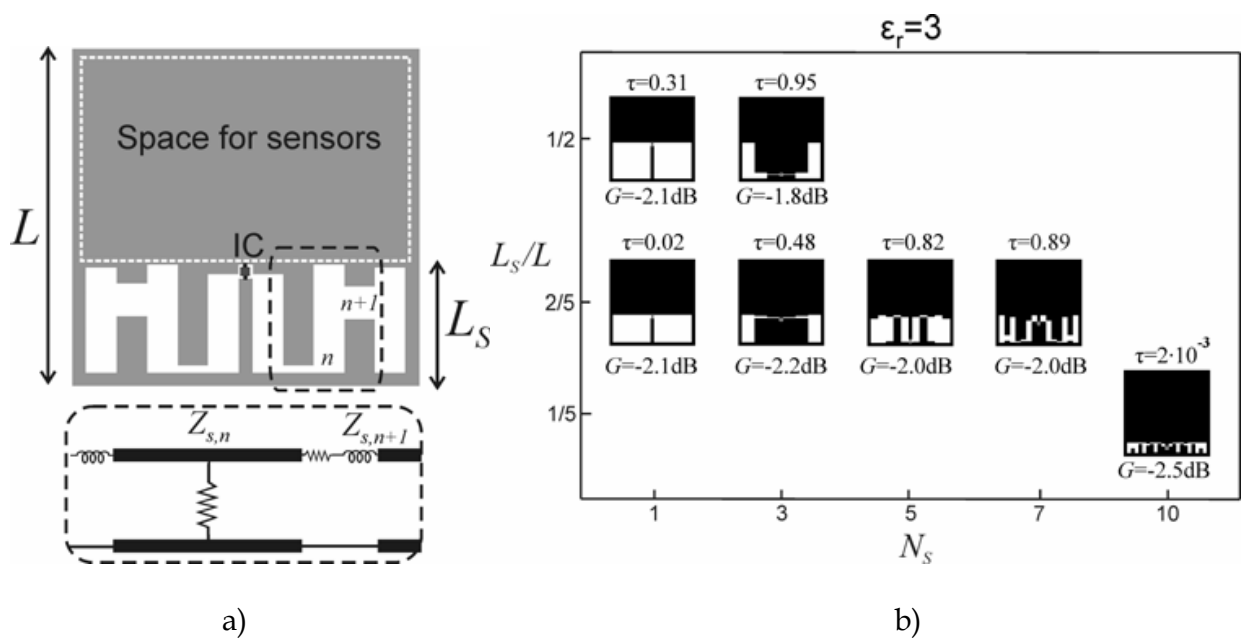
Fig. 8. Meandered Slot Antenna (MSA) tag. a) Layout and slot-line model. b) Examples with L=5cm, placed over a ε_r=3 dielectric half-space, which have been optimized for an IC with Z_{chip}=15-j450Ω, for different sizes L_s of the antenna region and for different number N_s of slot-line sections. A symmetric layout is assumed and therefore N_s represents half the overall slot transitions. G is the maximum gain in the air half-space.
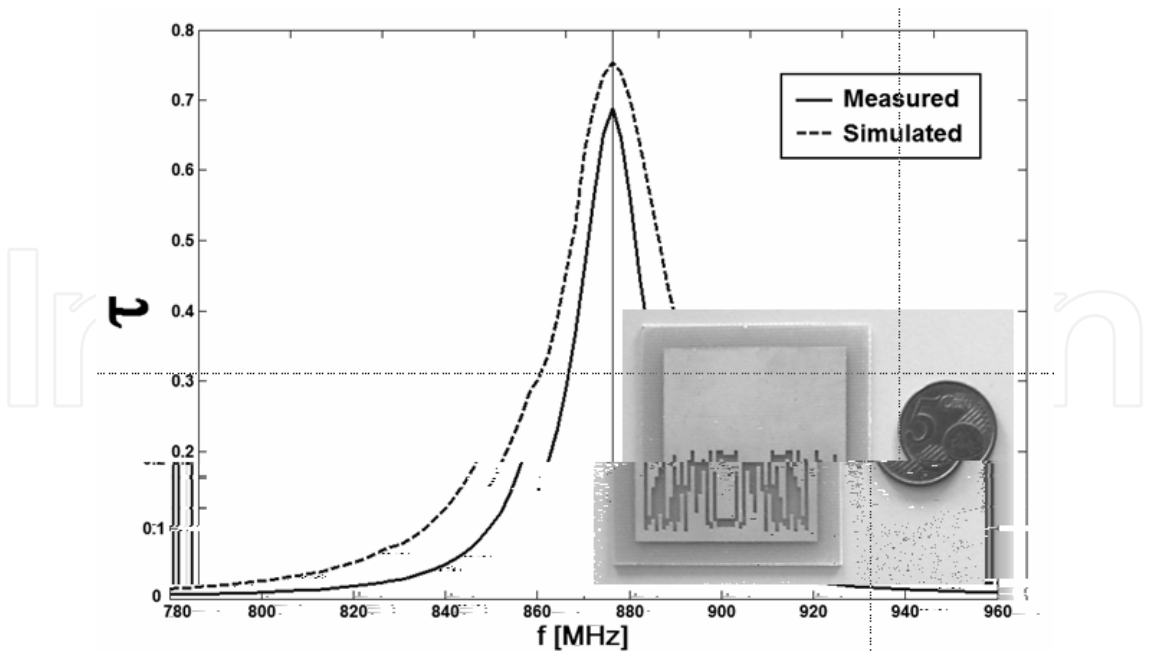
Fig. 9. MSA tag. Fabricated 5cm x 5cm prototype and in-air measurement of the power transmission coefficient.

4.2 Tag for non-contacting sensors

A further evolution of the slot-driven patch comprises an L-type patch folding (Fig. 10) with the purpose to increase the antenna radiation and in particular to reduce the power dissipation into the body district where the tag is placed. The folded region acts as a ground plane which partly isolates the antenna from the body. The radiation is now due to the H-slot itself, as in the previous layouts, but also to the current discontinuity in the folding and especially to the patch truncation. This configuration is referred to as *Slotted Clip Antenna* (SCA). When attached, for instance, onto a leg-like layered cylinder, this layout produces a larger gain than the NSSP and MSA tags, with maximum value of the order of 0dB with back radiation ranging within -10 ÷ -5dB. Fig. 11shows a fabricated prototype and the measured power transmission coefficient. The resulting read distance is sensibly improved in the front and at in the side regions of the antenna (Fig. 12).
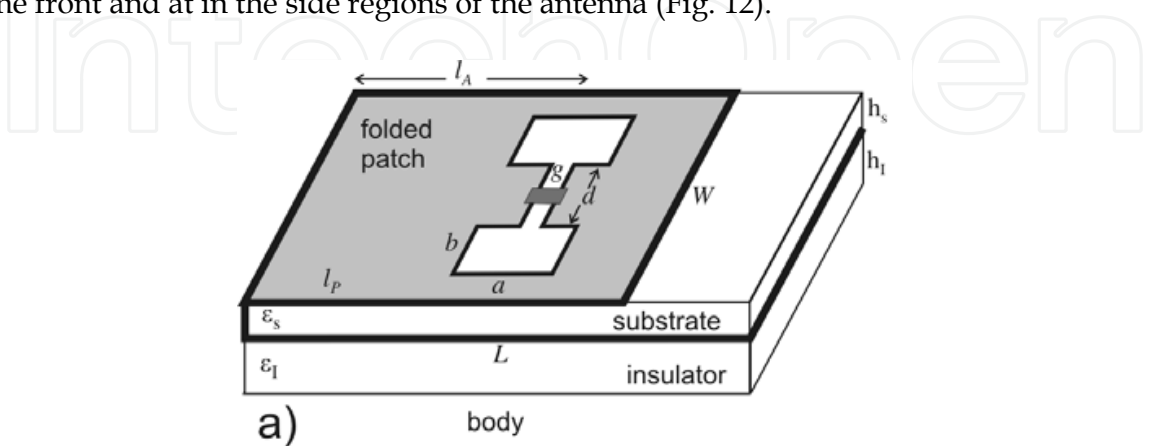

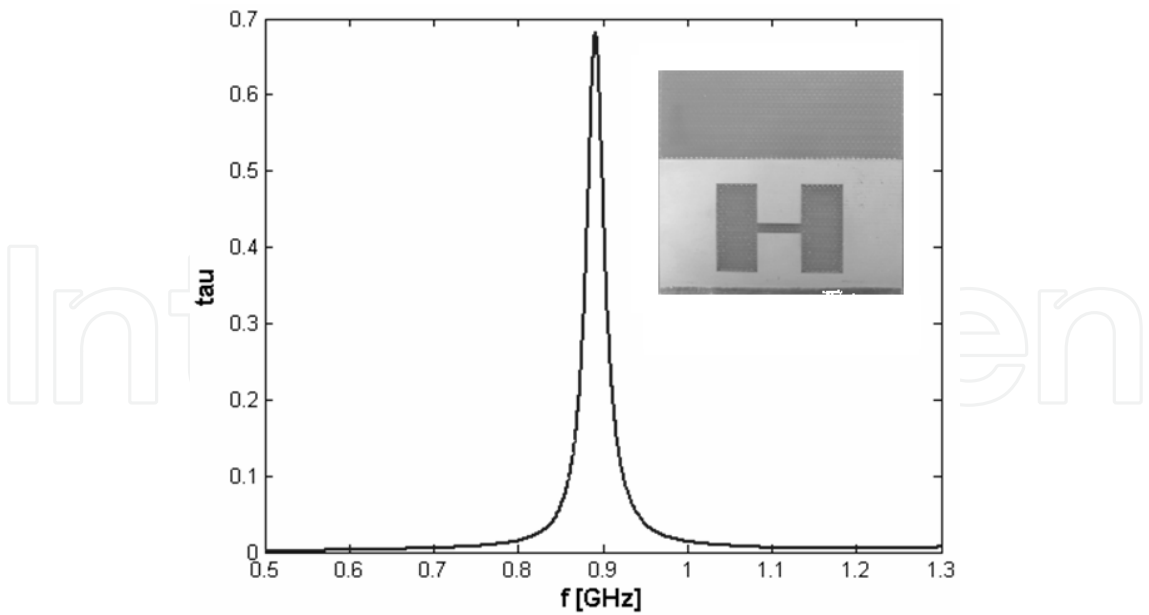Fig. 10. SCA tag. Layout of inverted slot antenna.

Fig. 11. SCA tag. Experimental prototype and measured power transmission coefficient for a microchip impedance Z_{chip}=10-j90 ohm.
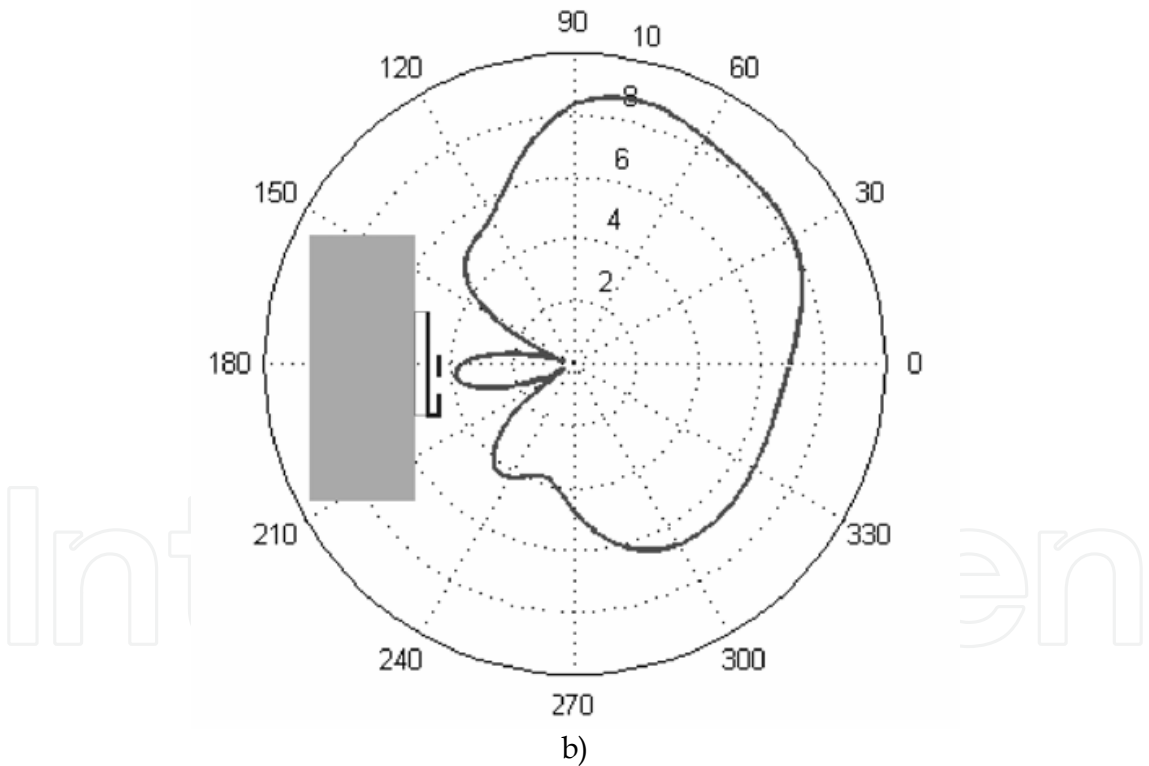

b)

Fig. 12. SILA Tag. Estimated activation distance for on-leg application when the reader emits 3.2 EIRP and the microchip has P_{chip}=10mW sensitivity.

4.3 An application example: monitoring the human motion

The SCA tag could be integrated with inertial switches for the monitoring of some Neural diseases such as the *Restless Legs Syndrome* (RLS) (Zucconi et al, 2006) and the *Periodic Limb Movements* (PLM). These sensor-motor disorders are clinically characterized by a compelling

urge to move the limbs, accompanied by uncomfortable and unpleasant sensations in the extremities. Symptoms show a characteristic circadian evolution with a nocturnal worsening leading to insomnia and consequently daytime sleepiness and reduced quality of life. The diseases can be diagnosed by polysomnography (PSG) or by movement recording using actigraphs.
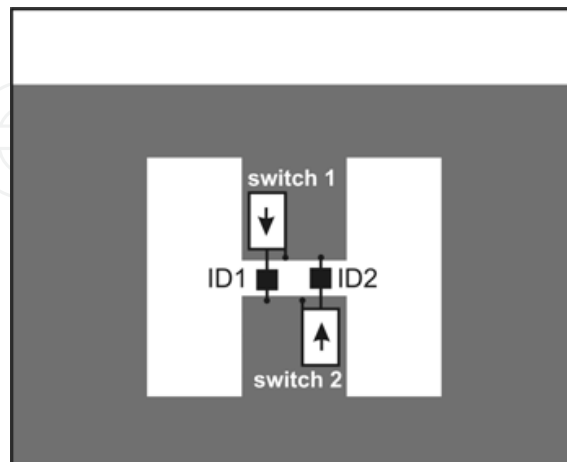

Fig. 13. Examples of integration between the SCA tag (front view), inertial switches (white boxes) and two microchips (black boxes). The arrows indicate the preferred direction of the switches.

The RFID technology offers interesting advantages over conventional diagnosis tools. The first one is the possibility to obtain very low-cost wireless devices, eventually single-usage, suited to be attached onto the body segments. Another interesting feature is that high-level aggregated data are easily achieved, just ready for the clinician.

In a possible set-up, one or more UHF RFID tags equipped with inertial switches will be attached onto the patient's limbs or onto other body regions. Depending on the verse of the applied acceleration, the switches react by changing their internal impedance from low (ideal short circuit) to high (ideally open circuit) impedance. A wireless one-axis sensor may be then achieved (Fig. 13) by means of a tag embedding two reverse-oriented inertial accelerometers, which turn between two RFID microchip transponder so that only one of the two possible IDs will be emitted (Fig. 13). Such an ID may be related to the acceleration's verse according to an ID modulation paradigm (Smith el al. 2005).

The tags are interrogated according to a proper repetition rate by an RFID reader placed at some place in the patient's room. The feasibility of this configuration is strictly correlated to the correct interrogation of the tags for any limbs position during the sleep within a typical hospital or domestic room, and with the compliance to the safety exposure regulations. In this perspective it is important to define the minimum features required to the body-antenna design, the number and the position of the tags, the sensibility of the inertial switches and the interrogation protocol.

A radio-mechanical model is introduced to simulate the biophysical signals collected by the reader during the legs motion, and to discuss the effect of other system parameters such as the inertial switch threshold and the interrogation rate. The model includes a simplified human phantom having 18 moving parts, individually controllable (Fig. 14.I). Some typical motion patterns in PLM episodes have been reconstructed by enforcing the trajectory of hip, knee and foot and calculated by a computer multi-body cinematic simulation solver. An

example of ID-modulated data received by the reader is shown in Fig. 14.I for different choices of the interrogation frequency. Each tag is able to correctly capture the dynamics in term of number of predicted PML frequency and approximate duration.
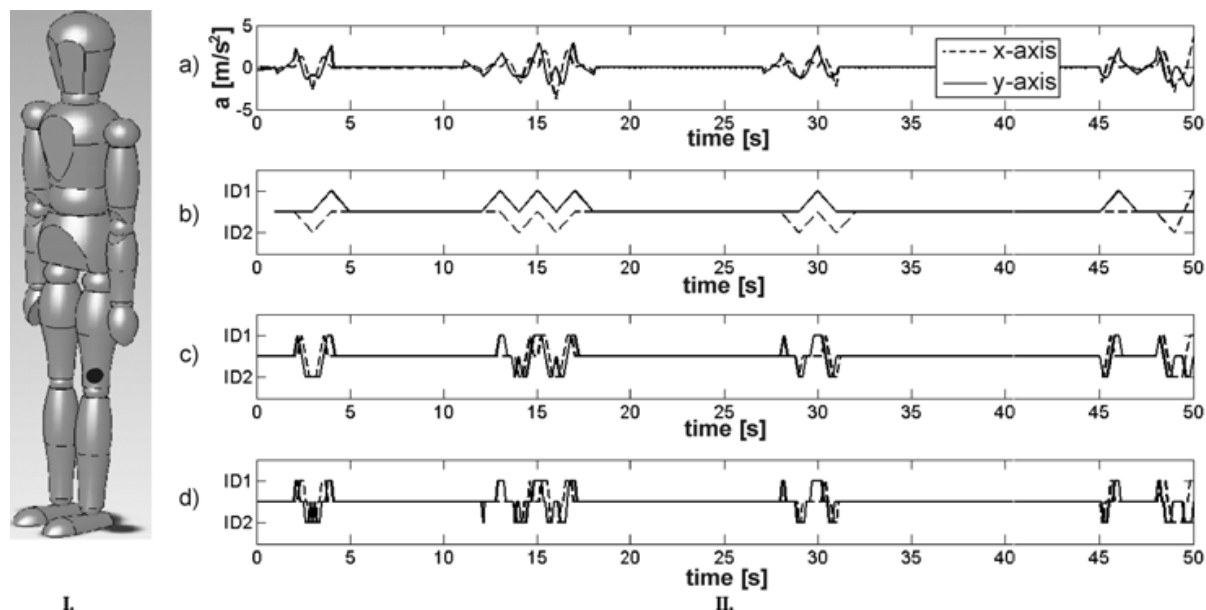

Fig. 14. I) Simplified human phantom. II) Leg's acceleration at the leg position marked by a black circle and ID-modulated received data for switch's acceleration threshold 0.1G and some interrogation frequency: b) f_C=1Hz; c) f_C=5Hz; d) f_C=10Hz.

5. Self-sensing RFID tags

Like any antenna immersed or located close to a real object, the input and radiation characteristics of a passive RFID transponder placed on a target, as well as the strength of the back-scattered power, are closely related to the physical properties of the tagged object itself, e.g. on its constitutive material, shape, temperature, humidity or other. Let Ψ denote the set of the relevant target's features which could undergo changes along with the time, or could have to be monitored in someway. If the tag antenna has been designed for optimal performances when placed on a target with nominal set of features Ψ_T, e.g. such that the antenna impedance $Z_A(\Psi)$ equals in this condition Z_{chip}^*, a change of one or more target's parameters with respect to Ψ_T may produce a variation of the input impedance and hence the mismatch $Z_A \neq Z_{chip}^*$. Accordingly, also the back-scattered power collected at the reader port will be modified (Fig. 15). In the limiting case, the tag may be completely mismatched so that $P_{R\to T} < p_T$ and the tag is therefore inactive. For the sake of clarity, let us focus on the simplified case for which a single target's feature is subjected to change, and such a parameter be the relative dielectric permittivity (simply permittivity ε in the following). It is now useful to define the tag's *Activation Band* $A_\varepsilon(d)$ for a link length d, as the set of target's permittivity values for which the power harvested by the tag is enough to activate it: $A(d) = \left\{\varepsilon \mid P_{R\to T}(d,\varepsilon) \geq p_T\right\}$.

As suggested by equation (3), if the reader-tag distance were known, the change in the target permittivity could be theoretically detected by monitoring the power back-scattered

by the transponder. Nevertheless, a single received data is not adequate to retrieve permittivity information in case of moving objects, or in applications in which the distance and the orientation of the tag with respect to the reader are not a-priori known (non-cooperative targets). To overcome these uncertainties, multiple independent back-scattered signals have to be collected by the reader. In the proposed platform, these signals are originated (Fig. 16) from either a *cluster* of N tags co-located onto a same target, or from a single tag provided with N input ports under the condition that each port or antenna has a different input impedance. In particular, we denote with $G_{T,n}$ the embedded radiation gain when only the nth port is fed and the others are connected to a reference load, and with $Z_{A,n}$ the input impedance at the nth port in the same conditions. Each port will be characterized by its Activation Band $A_{n,\varepsilon}(d)$.
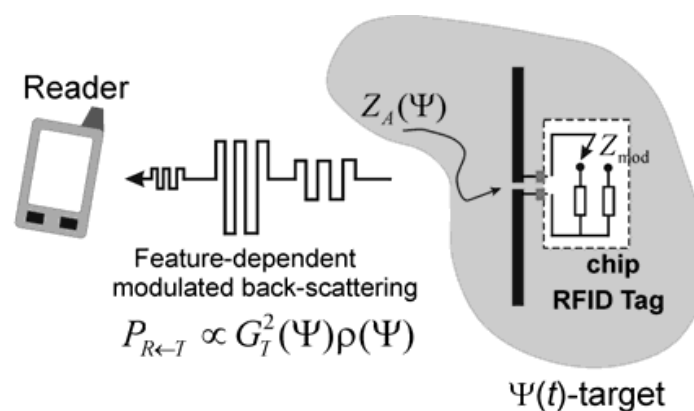

Fig. 15. Reader-tag scenario wherein the change of the target's features may produce a modulation of the backscattered power signal.
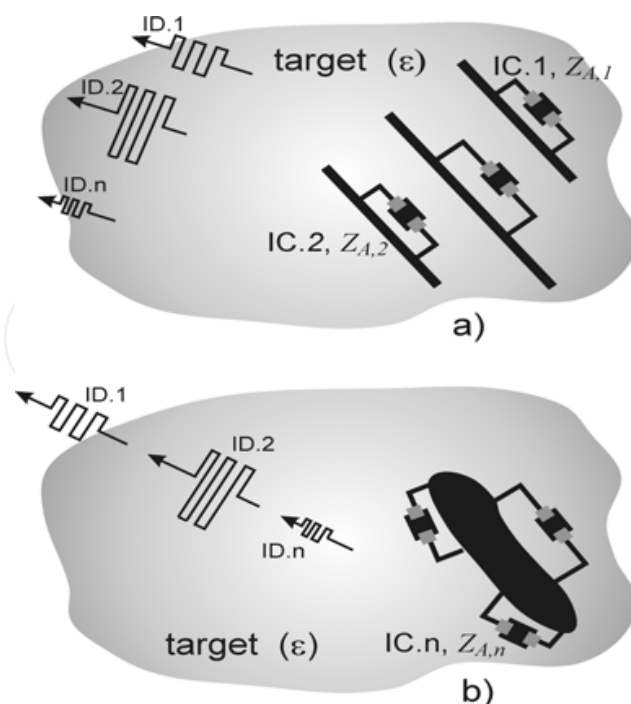

Fig. 16. Multi-port tag systems: a) a cluster of co-located single-port tags; b) a single multi-port tag provided with multiple chips.

The multi-port system has to be designed so that, having fixed a target geometry and having chosen N different *reference permittivities* $\{\varepsilon_1, \varepsilon_2, \ .. \ , \varepsilon_N\}$, the n th port impedance is matched to the microchip if the target's permittivity value is ε_n (e.g. $Z_{A,n}(\varepsilon_n) = Z^*_{chip}$). It means that, when the multi-chip system is placed on a real target, the ports will be differently mismatched ($Z_{A,n}(\varepsilon) \neq Z^*_{chip}$) and therefore they will originate independent back-scattered power signals, all of them carrying information about the target's permittivity. The resulting overall object is a *multi-port Sensor RFID (S-RFID) tag* that employs the same fabrication technology as the conventional RFID tags but, as shown later on, adds specific sensing capabilities to the typical identification features.

5.1 Sensing the target's permittivity

Depending on the link length d and on the particular design of the multi-port S-RFID tag, there will exist ranges of the target's permittivity for which either multiple ICs respond (overlapping of Activation Bands) and hence the reader is able to collect multiple backscattered signals, or only a port is at most activated and the reader may receive a single ID. Two different sensing modes can be correspondingly achieved: *analog sensing* (multiple responding ICs) and *discrete sensing* or *classification* (single responding IC). For both the cases, it is useful to introduce the *Sensing range* $\mathbf{S}(d)$ of the multi-port S-RFID tag, as *the set of all the possible values of the target's permittivity which could be detected, in some way, at a distance d*. The only analog sensing capability is here described, while a the complete theory could be find in (Marrocco et al., 2008).

If the tag has been designed for close reference permittivities { ε_n }, the port impedances will have similar (but not identical) power transmission coefficients τ_n so that multiple microchips will be turned on. In this case the multi-port system will have overlapped Activation Bands $\cap A_n \neq 0$. For any couplet of back-scattered signals received by the reader, each with a different modulation parameter $\rho_n(\varepsilon)$, it is possible to drop out the unknown reader-tag distance by calculating the *backscattered power ratio* $p_{i,j}$ between the received powers in equation (4),

$$p_{i,j}(\theta, \phi, \varepsilon) = \frac{P_{R \leftarrow T,i}(d, \varepsilon)}{P_{R \leftarrow T,j}(d, \varepsilon)} = \left[\frac{G_{T,i}(\theta, \phi, \varepsilon)}{G_{T,j}(\theta, \phi, \varepsilon)} \right]^2 \frac{\rho_i(\varepsilon)}{\rho_j(\varepsilon)} \tag{8}$$

However, $p_{i,j}$ is still affected by the uncertainty on the tag orientation (θ, ϕ) with respect to the reader. The multi-port tag design is therefore required to satisfy the condition of proportional gain patterns, e.g. such that $G_{T,i}(\theta, \phi, \varepsilon) / G_{T,j}(\theta, \phi, \varepsilon) = f(\varepsilon)$. This condition could be roughly satisfied considering a cluster of two antennas having a similar geometry.

The retrieval procedure is now described by means of an example involving a two-port system, e.g. able to backscatter two different IDs toward the reader. An overlapping configuration between the activation ranges is illustrated in Fig. 17. When both the ID_1 and the ID_2 are received by the reader, the unknown target dielectric permittivity ε_T will belong to the intersection of the two Activation Bands, e.g. $\varepsilon_T \in [A_1 \cap A_2]$, and therefore the p_{12} ratio can be calculated as in (8). The value of the target's permittivity is hence retrieved by using a *calibration curve* $\varepsilon(p_{12})$ which associates a target's permittivity to the actual

backscattered power ratio, measured by the reader, (Fig. 18). Such a $p_{12} \to \varepsilon_T$ relationship is specific for the particular application, e.g. for a particular class (geometry) of targets and needs to be produced off-line through measurements or numerical simulations on simplified, or well representative, target models by operating a sweep of the parameter under observation and calculating the resulting backscattered power ratio. The application of such a technique therefore requires preliminary electromagnetic processing to produce calibration curves for the specific class of objects and the so obtained database, together with the retrieval procedure, have to be embedded in the reader's (post)processing unit. The S-RFID range $\mathbf{S}(d)$ is given by the merging of the Activation Bands shared by couplets of ports: $S(d) = \{d: \quad A_m(d) \cap A_n(d) \neq 0\}$.
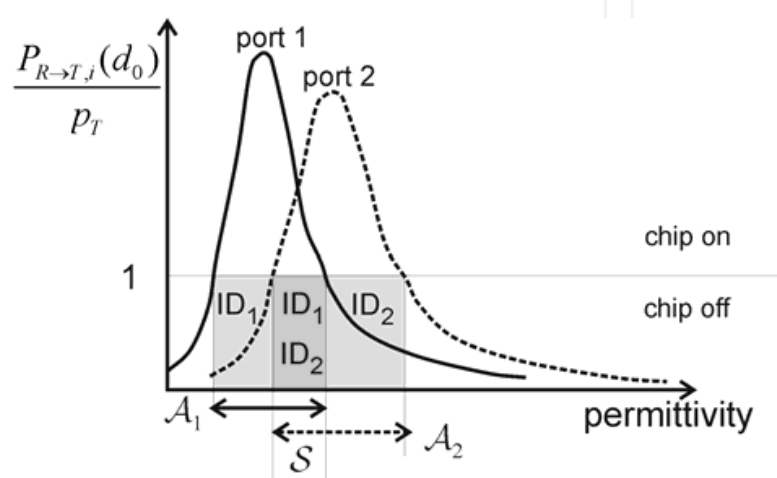
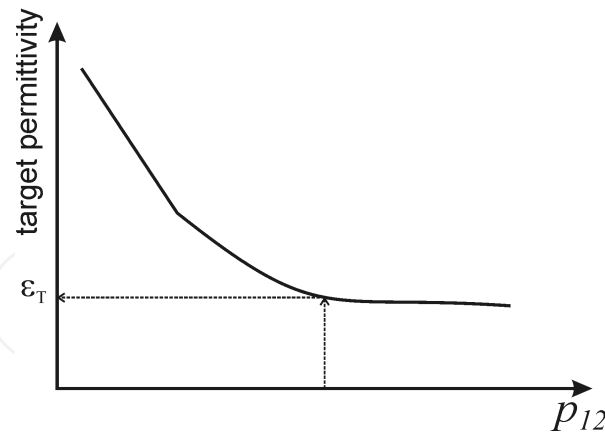Fig. 17. Typical Activation Bands, and Sensing Range, of a two-ports RFID tag, designed to work in analog-sensing mode.

Fig. 18. Example of calibration curves $\varepsilon(p_{ij})$ relating the measured backscattered power ratio to a target's permittivity value.

5.2 An experiment: sensing the filling percentage of a container

A very preliminary laboratory experiment is here discussed. The purpose is to demonstrate the validity of the basic principle concerning the possibility to govern the variation of the two-port tag antenna features with respect to the change of a real tagged body. A two-MLA (Meander Line Antennas) tag (Marrocco, 2003) has been designed for the sensing of the

filling level, *h*, of a box (Fig. 19). The variation of the shape of the target modifies the apparent permittivity sensed by the antennas and hence all their relevant parameters. With the aim to isolate and characterize the response of the antennas themselves, the experiment does not consider the RFID chip mounted on, and only the port impedances have been checked.

The target is again the perspex cubic box already used in Fig. 5, now filled up to a height *h* (changed during the experiment) by sugar powder (ε_r=3, σ=0). The box is placed over a large copper sheet (1m × 1m) acting as an image plane.
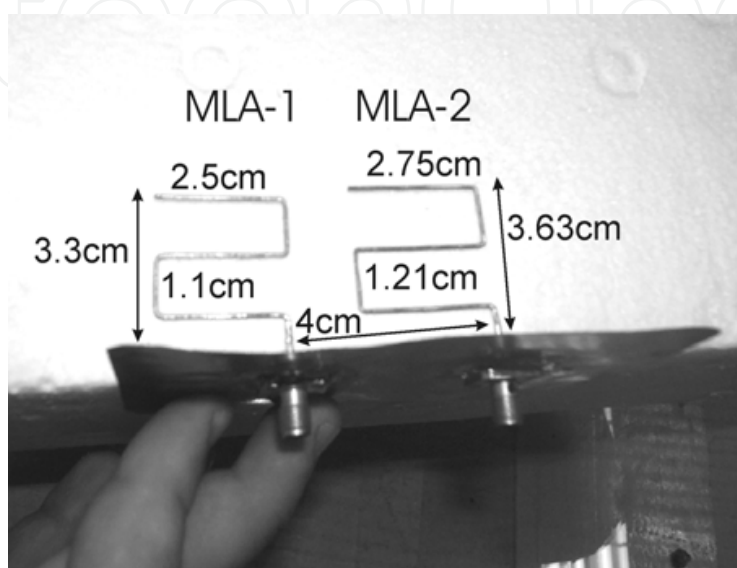
Fig. 19. Powder level sensing: meander-line-antennas prototype. Only half the structure is considered since the copper ground plane acts as an image plane.

The two MLAs are intended to be placed vertically on the external side of the box. Due to the presence of the ground plane, monopole configurations have been considered. Consequently, the impedance measurement results greatly simplified since no balun device is required. The antennas have regular meanders and they have been optimized for the best τ such that the MLA_1 and MLA_2 are matched, at 870MHz, to the microchip (Z_{chip}=50-j200Ω) when the sugar level is *h*=10cm and *h*=0cm (empty box), respectively. The two MLAs are scaled replicas. The overall antenna heights are 3.3cm and 3.63cm, respectively. The distance between the MLAs' gaps is 4cm. The tag prototype has been fabricated by 1mm-radius copper wire, and is shown in Fig. 19. The MLA monopoles are terminated on SMA connectors soldered on a 10cm copper sheet which is then placed in front of the perspex box as indicated in Fig. 20. At this purpose, the large ground plane was properly drilled to accommodate the SMA connectors for the connection to the HP 8753C Vector Network Analyzer by means of flexible coaxial cables.

The self-impedances Z_{11} and Z_{22} of the two-port tag are measured, having de-embedded the SMA connectors, when the filling level is increased in the range 0<*h*<10cm with steps of 2cm. The measurements are repeated in the reverse order (by emptying the box) and the two resulting sets of data finally averaged.

The resulting matching diagram of the power transmission factor, estimated by FDTD and measured, is shown in Fig. 21. It is possible to appreciate, beside the nice agreement between simulations and measurements, that the τ-curves are monotonic with the change of *h* and that each port is rather mismatched in the condition for which the other one exhibits unitary τ.
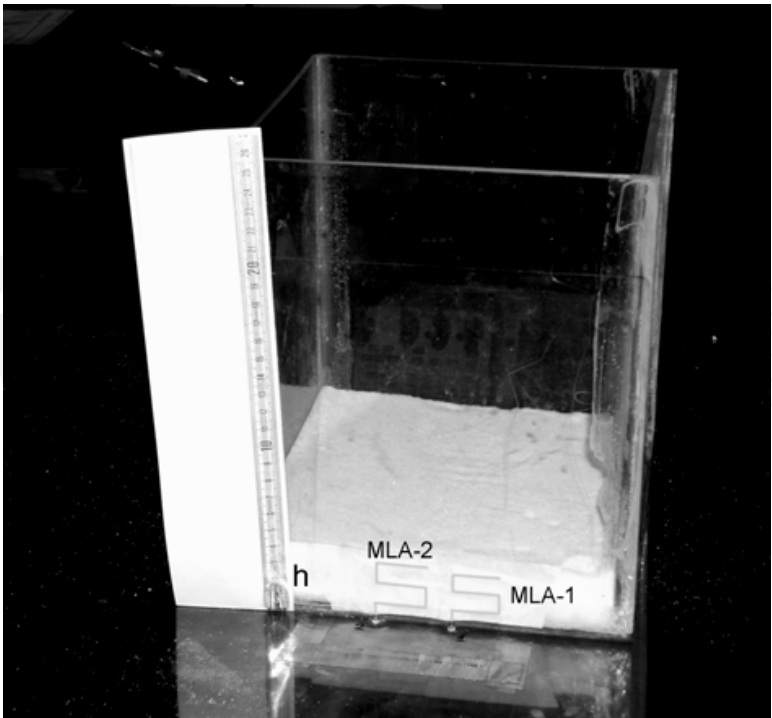
Fig. 20. Powder level sensing: experimental set-up comprising the two-MLA tags and a perspex cubic box of 20cm by 20cm cross-section partially filled with sugar up to a level h. The antennas are fixed to the box's vertical side by means of an adhesive ribbon.
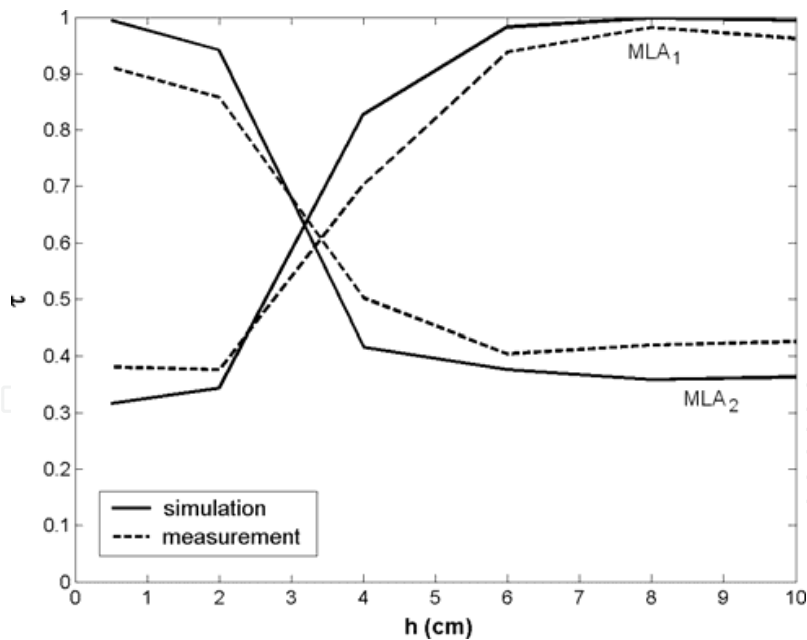

Fig. 21. Powder level: theoretical (simulated) and measured power transmission coefficients for the MLA$_1$ optimized for h=10cm, and MLA$_2$, optimized for an empty box (h=0).

The sensing effectiveness of the two-port tag depends on the calibration curve $p_{21} \leftrightarrow h$, and on the ratio in (8). The calibration curve $p_{21} \leftrightarrow \rho_1/\rho_2$ is monotonic, except for a very early short part with a good dynamic ($1 < p_{21} < 5$) when $2 < h < 8$. A saturation effect is clearly visible for levels higher than h=8cm, e.g. when the powder level greatly exceeds the vertical height of the

antennas. In this condition, a further increase in *h* does not produce additional variation of the antenna responses and such a change of the target could not be sensed since the sugar powder acts as an infinite medium for the two antennas. The sensed dynamic of the powder level could be increased by designing longer tags or using a vertical arrays of properly tuned tags.
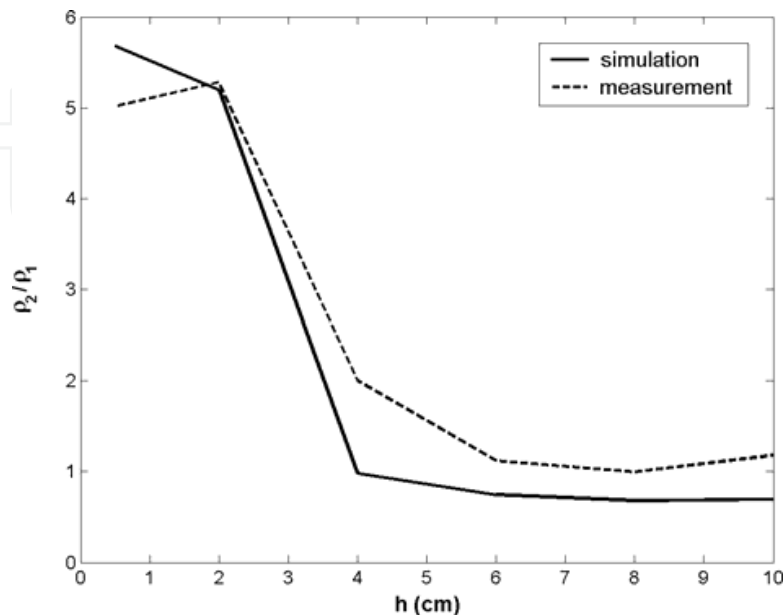

Fig. 22. Powder level: theoretical (simulated) and measured ρ_2/ρ_1 coefficients versus the sugar level h inside the box.

6. Conclusions

Designing low-cost antennas for sensing applications is still a great challenge, especially when the human body is involved. We are just at the beginning of the story and there is a significant margin of progress, both methodology, technological and experimental, to pursue in the next years. The reviewed tag configurations are only some of the many viable geometrical and electrical solutions, and are interesting for the relevant number of degrees of freedom and for the matching agility over different microchips and conditions.

Since the power consumption of the microchip transponder is continuously reducing, with a trend similar to the increase in the transistors' density in a chip (say the Moore Law), the concurrent research on antenna design, the use of smart materials embedding also sensorial capability, permits to figure out new classed of distributed and massive applications, mapping the physical phenomena into a virtual reality context, accessible from anywhere.

7. Acknowledgment

8. References

Calabrese C., Marrocco G. (2008), Meandered-Slot Antennas for Sensor-RFID Tags, *IEEE Antennas and Wireless Propagation Letters*, Vol.7, N.1, Jan. 2008, pp. 5-8

Cheng-Ju L., Li L. Shi-Zong C., Chi Chen W. (2004), Chun-Huang W., Xin-Mei C., Mobile healthcare service system using RFID, *Proceedings of IEEE Int. Conf. Networking Sensing and Control 2004*, Vol.2, 2004, pp.1014-1019

Chong C.Y., Kumar S. (2003), Sensor Networks: Evolution, Opportunities and Challenges, *Proceedings of the IEEE*, Vol. 91, N.8, Aug. 2003, pp. 1247- 1256

Curty J., Joehl N., Dehollain C., Delercq M. J. (2005), Remotely powered addressable UHF RFID integrated system, *IEEE J. Solid-State Circuits*, Vol.40, N.11, Nov. 2005, pp. 2193-2202

Gabriel C., Gabriel S., Corthout E., The dielectric properties of biological tissues: I. Literature survey," *Phys. Med., Biol.*, Vol. 41, No. 11, Nov. 1996, pp. 2231-2249

Lorincz K., Malan D.J., Fulford-Jones T.R.F., Nawoj A., Clavel A., Shnayder V., Mainland G., Welsh M., Moulton S. (2004), Sensor Networks for Emergency Response: Challenges and Opportunities, *IEEE Pervasive Computing*, Vol. 3, No. 4, Oct 2004, pp. 16-23

M. J. Ackerman M. J. (1998), The visible human project, *Proceedings of the IEEE*. Vol.86, N.3, 1998, pp. 504-511

Marrocco G. Bardati F. (1999), BEST a finite-difference solver for time electromagnetics, *Simulation Practice Theory*, Vol.7, No.3, May 1999, pp. 279-293

Marrocco G. (2007), Rfid antennas for the UHF remote monitoring of Human subjects, *IEEE Transaction on. Antennas and Propagation*, Vol.55, N. 6, June 2007, pp. 1862-1870

Marrocco G. (2008), The art of UHF RFID antenna design: impedance matching and size-reduction techniques, *IEEE Antennas and Propagation Magaz.*, Vol.50, N.1, Feb. 2008, pp.66-79

Marrocco G., (2003), Gain-optimized self-resonant meander line antennas for RFID applications, *IEEE Antennas Wireless Propag. Lett.*, Vol. 2, 2003, pp. 302–305

Marrocco G., Mattioni L., Calabrese C. (2008), Multi-port sensor RFIDs for wireless passive sensing of objects – basic theory and early results", *IEEE Trans. Antennas Propagat.*, Vol.58, N.8 Part2, Aug. 2008, pp 2691-2702

Nikitin P.V., Rao K.V.S. (2006), Theory and Measurement of Backscattering from RFID Tags, *IEEE Antennas and Propagation Magazine*, Vol. 48, No. 6, Dec 2006. pp. 212-218

Reindl L.M., Pohl A., Scholl G., Weigel R. (2001), SAW-Based Radio Sensor Systems, *IEEE Sensors Journal*, Vol. 1, No. 1, Jun 2001, pp. 69-77,

Sample A.P., Yeager D.J., Powledge P.S., Smith J.R. (2007), Design of a Passively-Powered, Programmable Sensing Platform for UHF RFID Systems, *Proceedings of IEEE International Conference on RFID*, Mar, 2007, pp. 149-156

Smith J.R., Jiang B., Roy S., Philipose M., Sundara-Rajan K., Mamishev K. (2005), ID modulation: Embedding sensor data in an RFID Timeseries, *Lecture Notes in Computer Science*, Vol. 3727, Nov. 2005, pp. 234-246

Taflove A. (1998), *Advances in Computational Electromagnetics: The Finite Difference Method*. Norwood, MA, Artech House, 1998.

Weile D. S., Michielssen E. (1997), Genetic algorithm optimization applied to electromagnetics: A review, *IEEE Trans. Antennas Propag.*, Vol. 45, No. 3, Mar. 1997, pp. 343–353

Zucconi M., Ferri R., Allen R., Baier P. C., Bruni O. (2006), The official World Association of Sleep Medicine (WASM) standards for recording and scoring periodic leg movements in sleep (PLMS) and wakefulness (PLMW), *Sleep Medicine*, N.7, July 2006, pp. 175-183

Development and Implementation of RFID Technology

Edited by Cristina Turcu

The book generously covers a wide range of aspects and issues related to RFID systems, namely the design of RFID antennas, RFID readers and the variety of tags (e.g. UHF tags for sensing applications, surface acoustic wave RFID tags, smart RFID tags), complex RFID systems, security and privacy issues in RFID applications, as well as the selection of encryption algorithms. The book offers new insights, solutions and ideas for the design of efficient RFID architectures and applications. While not pretending to be comprehensive, its wide coverage may be appropriate not only for RFID novices but also for experienced technical professionals and RFID aficionados.

How to reference

In order to correctly reference this scholarly work, feel free to copy and paste the following:

Gaetano Marrocco (2009). UHF Tags for Sensing Applications, Development and Implementation of RFID Technology, Cristina Turcu (Ed.), ISBN: 978-3-902613-54-7, InTech, Available from: http://www.intechopen.com/books/development_and_implementation_of_rfid_technology/uhf_tags_for_sensing_applications

INTECH
open science | open minds